# Preparation of yolk–shell microspheres as temperature switch on/off catalysts

*Kun Yang[1], Zhao Dai[1], Yuanyuan Chu[1], Guangping Chen[2]*

*[1]State Key Laboratory of Hollow Fiber Membrane Material and Process, School of Environmental and Chemical Engineering, Tianjin Polytechnic University, Tianjin300387, People's Republic of China*
*[2]Department of Physiological Sciences, College of Veterinary Medicine, Oklahoma State University, Stillwater OK 74078, USA*
*E-mail: daizhao@gmail.com*

Published in Micro & Nano Letters; Received on 8th October 2015; Revised on 30th November 2015; Accepted on 2nd December 2015

A novel kind of yolk–shell microspheres was presented in this Letter. First, 250 nm of magnetic $Fe_3O_4$ nanoparticles was prepared by solvothermal reaction. Then, the $Fe_3O_4$ particles were coated with Au nanoparticles (AuNPs), $SiO_2$, and poly(N-isopropylacrylamide) (PNIPAM). After the removal of the $SiO_2$ layer by etching with HF solution, the yolk–shell microspheres were prepared. Each yolk–shell microsphere had a movable core ($Fe_3O_4$ self-assembled AuNPs) and temperature-responsive shell (PNIPAM). The yolk–shell structure of these microspheres was confirmed by transmission electron microscopy and Fourier-transform infrared spectroscopy. The catalytic performances of these yolk–shell microspheres were investigated under different environmental temperatures. The results indicated that the reduction from 4-nitrophenol to 4-aminophenol by $NaBH_4$ was slowed when the temperature was increased because of the hydrophobic and the shrinking sate of PNIPAM shell and the yolk–shell microspheres had a characteristic of temperature switch on/off when the cross-linking degree was about 20%.

**1. Introduction:** As a new category of structured materials, hollow particles have gained increasing attention owing to their potential applications such as low density, high specific area, good flow ability, and surface permeability [1, 2]. They have found wide applications in many fields, such as catalysis, drug and gene delivery, hydrogen storage, and artificial cells [3, 4]. Different with the traditional hollow or core–shell microspheres, a yolk–shell microsphere is the hybrid of core–shell and hollow structures with a distinctive core/void/shell configuration and therefore the core is movable in the hollow shell [5, 6]. Since yolk–shell microspheres can have differently functional shells and cores, they have various applications in catalysis, batteries, and biomedical fields [7, 8]. The usual method for the preparation of yolk–shell particles is based on the template-assisted method [9–12]. First, a core [e.g. Au nanoparticle (AuNP)] particle is prepared and then coated with a polymer or a $SiO_2$ layer. This layer is further functionalised with certain reactive groups to grow another shell. After removal of the middle layer, a yolk–shell particle is prepared. Usually, most of the reported works are focused on the functional cores [11, 13]. Nanoparticles such as tin [14], gold [10, 12], or metal oxides [15] could be incorporated into the hollow microspheres and novel properties can be introduced to the hollow microspheres. Wan *et al*. [14] synthesised tin nanoparticles encapsulated in elastic hollow carbon spheres with uniform size, in which tin nanoparticles with a diameter <100 nm were encapsulated in one thin hollow carbon sphere. Zhang and co-workers [10] reported yolk–shell microspheres containing a single AuNP core (21–50 nm) and a mesoporous shell of hollow mesoporous silica microspheres (about 200 nm) and investigated the size-dependent activity of the AuNP core when the yolk–shell microspheres were as the catalyst. Yang and co-workers [12] prepared a poly(*N*, *N*′-methylenebisacrylamide) (PMBAAm) yolk–shell microsphere (about 50–100 nm) with a movable AuNP core (about 13 nm) by the selective etching of the silica middle layer in hydrofluoric acid. The yolk–shell microsphere with a single noble metal nanoparticle core has a high stability in catalysis [16] and exhibit a high capacity and good cycle performance [6] because the coalescence tendency of metal nanoparticles can be avoided. However, the particle size of these yolk–shell microspheres is very small, which will result in the difficulty of the separation of yolk–shell microspheres from reaction system as well as the deformation and damage of the shell layer under ultracentrifugation.

Recently, the multifunctional hollow polymeric particles have a great improvement. Du and Liu [9] reported dually thermo and pH-responsive yolk/shell polymer microspheres as a drug delivery system when poly(methacrylic acid-*co*-ethyleneglycol dimethacrylate) [P(MAA-*co*-EGDMA)] microspheres as cores and poly(N-isopropylacrylamide-*co*-methacrylic acid) [P(NIPAM-*co*-MAA)] as shells. Poly(N-isopropylacrylamide) (PNIPAM) is a promising thermo-responsive polymer with a lower critical solution temperature (LCST) of about 32 °C in water, individual PNIPAM chain undergoes a phase transition from a hydrophilic, water-swollen state to a hydrophobic, globular state when heated above its LCST, as well as cross-linked PNIPAM gels [17]. Li *et al*. [18] reported the synthesis of the poly(methacrylamide) (PMAA)–PNIPAM double-walled concentric hollow microspheres, which display the response independently to changing pH and temperature. However, when the yolk–shell microspheres were used as the catalysts, the shells are usually used as the coat and support materials [19–21].

In this Letter, a novel kind of yolk–shell microspheres with large diameters is presented, when $Fe_3O_4$ nanoparticles self-assembled AuNPs ($Fe_3O_4$/Au) are as the multifunctional cores and PNIPAM as the temperature-sensitive shells. The $Fe_3O_4$/Au core can carry more AuNPs and be separated from reaction system easily because of the magnetic property of $Fe_3O_4$ particles. Moreover, the nanopoles of shells will switch off/on because of the temperature sensitivity of PNIPAM [22], which will affect the mass transfer pathways between the reaction system and hollow microspheres (Fig. 1). When the circumstance temperature is lower than LCST, the small molecule, 4-nitrophenol (4-NP), can cross the PNIPAM shell, approach the $Fe_3O_4$/Au cores and be reduced to 4-aminophenol (4-AP). Moreover, the increase of temperature will not increase the reaction rate, which is much different with the traditional catalysts, because of the switch off of the mass transfer pathway of PNIPAM shells.

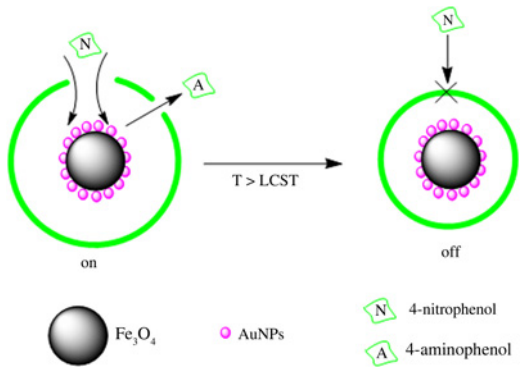


**Fig. 1** *Temperature switch on/off of the yolk–shell microspheres*

## 2. Materials and methods

2.1. Materials: $FeCl_3{\cdot}6H_2O$, trisodium citrate, sodium acetate anhydrous (NaAc), ethylene glycol, $HAuCl_4{\cdot}4H_2O$, sodium borohydride ($NaBH_4$), polyvinylpyrrolidone (PVP) K30 (MW ~30,000), hydrofluoric acid (HF) (40.0%), were analytical grade and purchased from Kermel Chemical Reagent Co. Ltd (Tianjin, China). Tetraethyl orthosilicate (TEOS), *N, N′*-methylenebisacrylamide (MBA), potassium persulphate (KPS), 3-aminopropyl triethylsilane (APTES), 3-(methacryloyloxy)propyl trimethoxysilane (MPS) were supplied by Aldrich-Sigma. 4-NP, *N*-isopropylacrylamide (NIPAM, 98.0%) was purchased from Tokyo Chemical Industry Co., Ltd and recrystallised from hexane. Deionised water was used in all experiments.

2.2. Synthesis of $Fe_3O_4$ particles: $FeCl_3{\cdot}6H_2O$ (2.70 g, 10.0 mmol), trisodium citrate (0.50 g, 1.70 mmol), and NaAc (5.40 g, 65.8 mmol) were dissolved in ethylene glycol (80 ml). The mixture was stirred vigorously for 1 h and then sealed with a Teflon-lined stainless-steel autoclave (150 ml capacity). The autoclave was heated to and maintained at 200°C for 12 h. The black products were washed with ethanol several times and dried under vacuum at 60°C for 8 h [23].

2.3. Synthesis of $Fe_3O_4$ self-assembled AuNPs ($Fe_3O_4$/Au): A 0.30 g of as-prepared $Fe_3O_4$ particles was homogeneously dispersed in a mixed solution of 140 ml of ethanol, 30 ml of deionised water, and 3.0 ml of ammonia aqueous solution (28%), then the mixture was subjected to mechanical stirring and sonication in a water bath. Subsequently, 10 ml of APTES (5 vol % in ethanol, containing 1 vol% TEOS) was added dropwise to the dispersion under continuous stirring and sonication. After 2 h, the sonication was stopped and kept stirring for 6 h. The product was collected by a magnet, washed several times with ethanol and water, and redispersed in 100 ml of water. AuNPs were

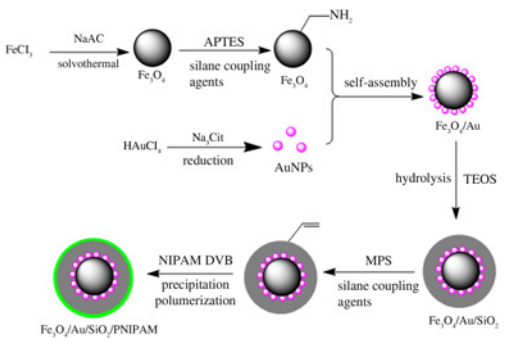


**Fig. 2** *Schematic illustration of preparation of $Fe_3O_4$/Au/$SiO_2$/PNIPAM composite microspheres*

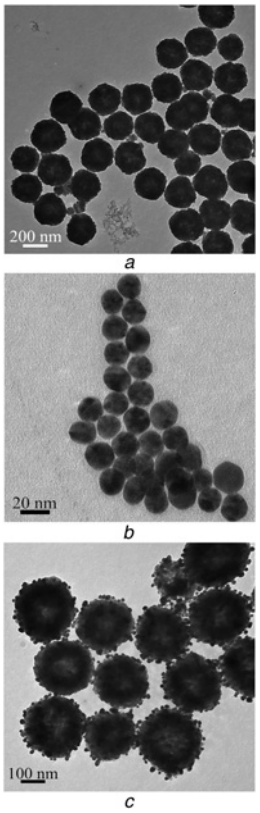


**Fig. 3** *TEM images of*
*a* $Fe_3O_4$
*b* AuNPs
*c* $Fe_3O_4$/Au particles

prepared according to Fren's method [24]. After centrifugation and collection, the modified $Fe_3O_4$ dispersion (100 ml) was mixed with 125 ml of AuNPs by vigorous stirring for 2 h. The formed $Fe_3O_4$/Au particles were then separated, washed several times with water and dried under vacuum at 60°C for 8 h.

2.4. Synthesis of $SiO_2$ coated $Fe_3O_4$/Au microspheres ($Fe_3O_4$/Au/$SiO_2$): A 25 ml of $Fe_3O_4$/Au suspension (0.2 wt% in water) was mixed with 25 ml of PVP solution (0.4 wt% in water) under sonication for 10 min, then separated and washed with water two times, subsequently, it was dispersed in a mixture of ethanol (100 ml), water (12 ml), ammonia solution (3 ml, 28%) and TEOS (0.6, 0.8, 1.0, and 1.2 ml, respectively). The mixture was stirred mildly for 2 h under sonication in a water bath. Then, 1.2 ml of MPS was added over a period of 18 h under continuous stirring. After the reaction, the product was collected, washed with ethanol and water several times, and redispersed in 25 ml of water for further uses [25].

2.5. Synthesis of NIPAM coated $Fe_3O_4$/Au/$SiO_2$ core/shell particles ($Fe_3O_4$/Au/$SiO_2$/NIPAM): A 25 ml of $Fe_3O_4$/Au/$SiO_2$ dispersion was mixed with 15 ml of aqueous solution containing 0.15 g of NIPAM and 0.015 g or 0.03 g of MBA by sonication. After being degassed with nitrogen for 20 min, the solution was heated up to 70°C, and 2 ml of KPS solution (3 mg/ml) was added to initiate the polymerisation. After stirring for 6 h, the product was collected and washed with water, and redispersed in deionised water (45 ml, ca. 0.3 wt%) for further uses.

2.6. Synthesis and catalytic performance of yolk–shell microspheres: The $SiO_2$ layer was etched by very low-concentration HF solution (ca. 0.1 wt%). The $Fe_3O_4$/Au/




doi: 10.1049/mnl.2015.0435

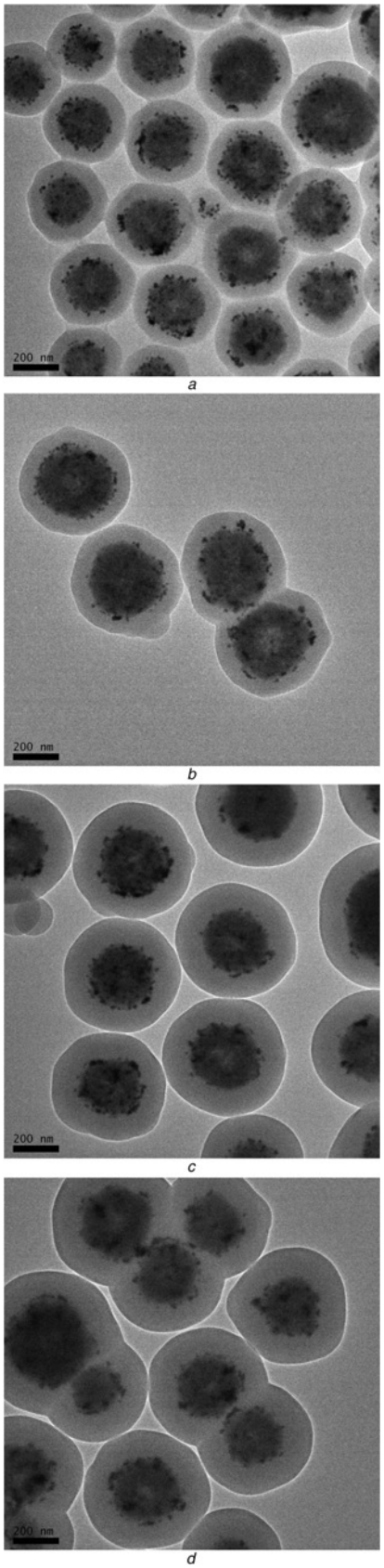


**Fig. 4** *TEM images of the $Fe_3O_4$/Au/$SiO_2$ microspheres with various $SiO_2$ shell thickness, the average thickness were*
*a* 54 nm
*b* 67.5 nm
*c* 105 nm
*d* 117.5 nm
All scale bars are 200 nm

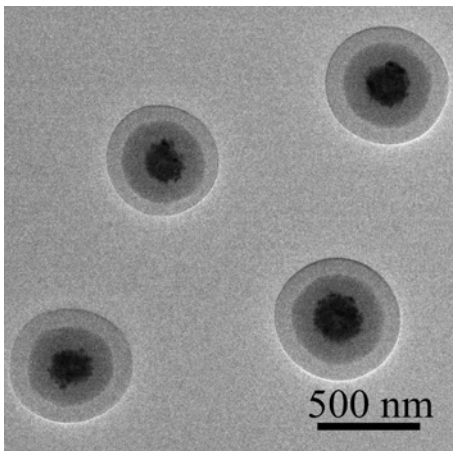


**Fig. 5** *TEM of $Fe_3O_4$/Au/$SiO_2$/PNIPAM composite microspheres*

$SiO_2$/PNIPAM aqueous dispersion (45 ml) was subjected to mechanical stirring (400 rpm), then added immediately 0.1 ml of HF solution, after stirring for 12min, another 0.1 ml of HF solution was added and the mixture was stirred for another 13–15 min. The resultant product ($Fe_3O_4$/Au/void/PNIPAM yolk–shell microspheres) was collected by a magnet and washed several times with water, and dispersed in 25 ml of water (ca. 0.3 wt%). The reduction of 4-NP by $NaBH_4$ was carried out in a quartz cuvette. Briefly, 0.015 ml of aqueous 4-NP solution (0.01 M), 0.2 ml of $NaBH_4$ solution (0.4 M) were mixed with 3 ml of deionised water in a quartz cuvette. Subsequently, 0.02 ml of aqueous dispersion of the yolk–shell microspheres (0.3 wt%) was added and the UV–vis spectra were measured by an Evolution-300 UV–vis spectrometer (ThermoFisher) equipped with a Peltier device for temperature controls at 25, 32, 45, and 55°C.

2.7. Reusability of yolk–shell microspheres: The cycle performances were investigated using yolk–shell microspheres with 20% cross-linking degree at 25°C with six cycle times. After each cycle, the catalysts were separated from the solution using a magnet, washed with water two times and redispersed into 1 ml deionised water.

## 3. Results and discussion

3.1. Synthesis of $Fe_3O_4$/Au/$SiO_2$/PNIPAM microspheres: The synthetic procedure for the $Fe_3O_4$/Au/$SiO_2$/PNIPAM multi-layered composite microspheres was shown schematically in Fig. 2. First, the magnetite $Fe_3O_4$ nanoparticles were prepared via a solvothermal reaction by reduction of $FeCl_3{\cdot}6H_2O$ under a high temperature with ethylene glycol as a reducing agent in the presence of NaAc and trisodium citrate [23]. Second, the magnetite $Fe_3O_4$ particles were functionalised by amino groups through simultaneous hydrolysis of APTES and TEOS. After the self-assembly of AuNPs on them, the $Fe_3O_4$/Au nanoparticles were obtained. Finally, a layer of silica was coated onto the $Fe_3O_4$/Au composite particles in the presence of PVP by Stöber method. For further polymerisation, MPS was used as a silane coupling agent to modify the surface of $Fe_3O_4$/Au/$SiO_2$ particles with vinyl groups. After the seed precipitation polymerisation with NIPAM monomer and MBA cross-linker, the $Fe_3O_4$/Au/$SiO_2$/PNIPAM microspheres were obtained.

The transmission electron microscopy (TEM) images were obtained by an H-7650 (Hitachi, Japan) or JEM-2100 (JEOL, Japan) transmission electron microscope. The results of $Fe_3O_4$, AuNPs, and $Fe_3O_4$/Au were shown in Fig. 3, which indicated that $Fe_3O_4$ particles had a nearly spherical shape and uniform size about 250 nm (Fig. 3*a*). In the reaction, NaAc was as the

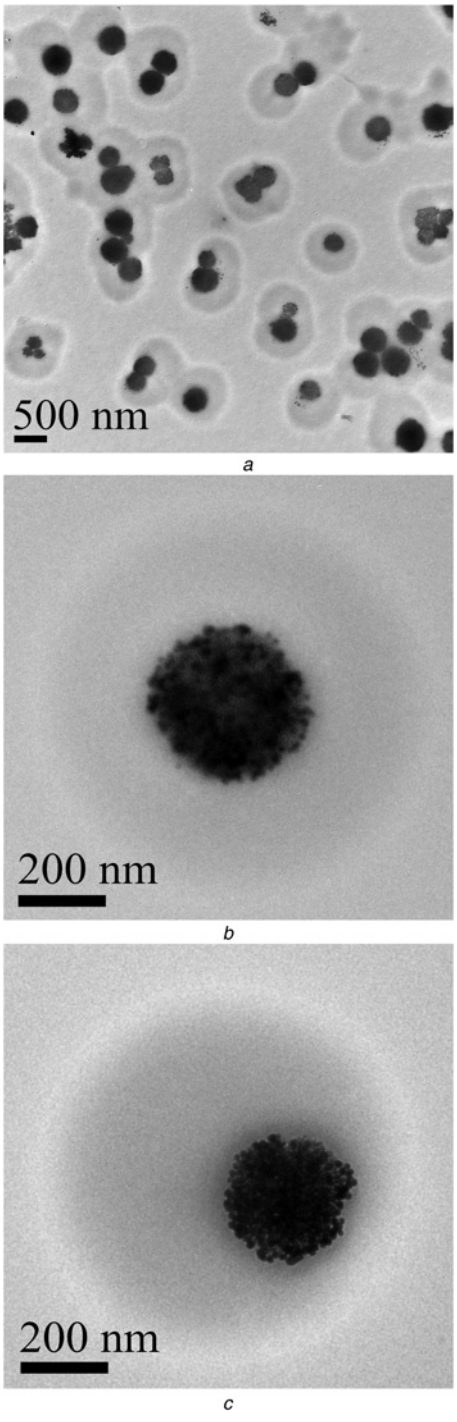


**Fig. 6** *TEM images of*
*a* $Fe_3O_4$/Au/void/PNIPAM yolk–shell microspheres
*b* Centricity core
*c* Eccentricity core

electrostatic stabilisation agent to prevent the coalescence of particles. Moreover, it could increase the alkalinity of reaction system and improve the hydrolysis of $FeCl_3$ to form $Fe(OH)_3$ which could be partially reduced into $Fe(OH)_2$ at a high temperature and finally form $Fe_3O_4$ nanoparticles through dehydration [26]. Trisodium citrate was as the reductant and stabiliser at the same time because three carboxylate groups of it had a strong coordination affinity to iorn(III) ions, which would result in the $Fe_3O_4$ particles exhibited excellent dispersibility in water and ethanol [26]. AuNPs also had a spherical shape and uniform size (about 16 nm in diameter) (Fig. 3*b*). They were also wrapped and stabilised by

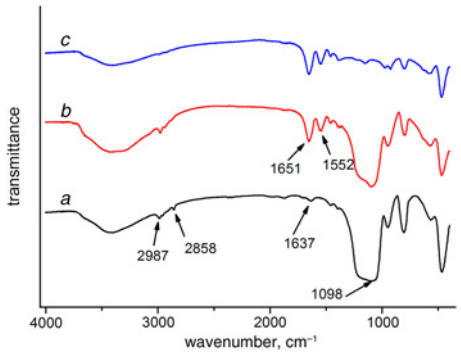


**Fig. 7** *FTIR spectra of*
*a* MPS modified $Fe_3O_4$/Au/$SiO_2$
*b* $Fe_3O_4$/Au/$SiO_2$/PNIPAM
*c* $Fe_3O_4$/Au/void/PNIPAM yolk–shell microspheres

citrate ion in water, which could result in the difficulty of the self-assembly of AuNPs on $Fe_3O_4$ ($Fe_3O_4$/AuNPs) particles because of the electrostatic repulsive force between AuNPs and $Fe_3O_4$ particles. Therefore, two kinds of silane coupling agents, APTES and TEOS (5:1, v/v), were utilised to endow abundant amino groups on the surface of $Fe_3O_4$ particles. These surface amino groups of $Fe_3O_4$ could react with AuNPs by coordination bonds [27] and result in AuNPs evenly covered the surface of $Fe_3O_4$ particles (Fig. 3*c*).

The encapsulation of $Fe_3O_4$/AuNPs with $SiO_2$ shell had two important advantages. First, the silica coating provided a large amount of terminated silanol, which could be modified with various active groups or ligands through well-developed silane chemistry. Second, the thickness of $SiO_2$ shell and size of composite microspheres could be easily tuned by adjusting the feeding amount of silica source (TEOS). However, it was difficult to coat $SiO_2$ directly on $Fe_2O_3$/AuNPs surfaces due to the low chemical affinity between AuNPs and $SiO_2$ from TEOS. Therefore, a coupling agent, PVP, was introduced to improve the formation of $SiO_2$ shell on the $Fe_2O_3$/AuNPs surfaces [25]. The thickness of $SiO_2$ shell could be controlled directly under different amount of TEOS (Fig. 4). When the TEOS amount was 0.6, 0.8, 1.0, and 1.2 ml, the average thickness of the corresponding $SiO_2$ shell was 54, 67.5, 105, and 117.5, respectively. The average thickness of $SiO_2$ shell and the feeding TEOS amount ($g$) had a linear tendency, which indicated that the hydrolysis rate of TEOS was a constant [26].

3.2. Preparation of $Fe_3O_4$/Au/$SiO_2$/PNIPAM microspheres: Various polymerisation methods such as atom transfer radical

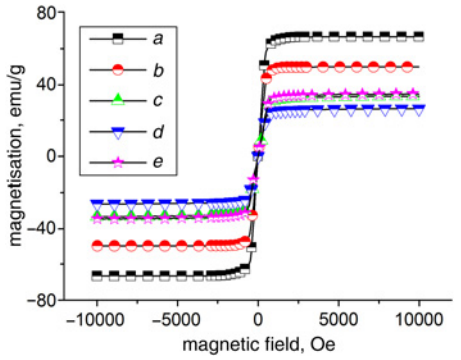


**Fig. 8** *Magnetic hysteresis curves of*
*a* $Fe_3O_4$
*b* $Fe_3O_4$/Au
*c* $Fe_3O_4$/Au/$SiO_2$
*d* $Fe_3O_4$/Au/$SiO_2$/PNIPAM
*e* $Fe_3O_4$/Au/void/PNIPAM yolk–shell microspheres




doi: 10.1049/mnl.2015.0435

polymerisation [28], reversible addition-fragmentation chain transfer polymerisation [29], and precipitation polymerisation [18, 30] can be used to coat $SiO_2$ with a polymer layer. Among these methods, precipitation polymerisation is convenient and easy to carry out [13, 19]. Before the polymerisation, $Fe_3O_4$/Au/$SiO_2$ microspheres were modified with vinyl groups by silane coupling agent MPS. The TEM results of $Fe_3O_4$/Au/$SiO_2$/PNIPAM microspheres were shown in Fig. 5 when $Fe_3O_4$/Au/$SiO_2$ microspheres with 105 nm thickness of $SiO_2$ shell (Fig. 4*c*) were as the seeds, which indicated that the composite microsphere with a multilayer structure had smooth and circular shape and the diameter was about 600 nm as well as the thickness of NIPAM shell was about 79 nm.

3.3. Preparation of yolk–shell microspheres: The $SiO_2$ layer of $Fe_3O_4$/Au/$SiO_2$/PNIPAM microsphere was etched in 0.1 wt% of HF solution to form $Fe_3O_4$/Au/void/PNIPAM yolk–shell microspheres (Fig. 6). The results indicated that each yolk–shell microsphere had a hollow structure with a movable core (Figs. 6*b* and *c*).

The Fourier-transform infrared (FTIR) spectra were collected on a Tensor-37 spectrometer (Bruker, Germany) and the results of MPS modified $Fe_3O_4$/Au/$SiO_2$, $Fe_3O_4$/Au/$SiO_2$/PNIPAM, and $Fe_3O_4$/Au/void/PNIPAM yolk–shell microspheres were shown in Fig. 7. The absorption peak at 1098 $cm^{-1}$ was assigned to the asymmetric stretching vibration of the Si–O–Si bonds, the absorption peak at 1637 $cm^{-1}$ was attributable to the vinyl groups of MPS [31, 32], the peaks at 2858 and 2987 $cm^{-1}$ were due to the vibration of the methylene and methyl groups, respectively, in MPS molecule (Fig. 7*a*) [31]. The absorption peaks at 1552 and 1651 $cm^{-1}$ associated with the amide groups of PNIPAM shell (Fig. 7*b*) [18]. After etching, the absorption peak at 1098 $cm^{-1}$ of $SiO_2$ was disappeared (Fig. 7*c*), which indicated the yolk–shell microspheres were obtained.

The magnetic hysteresis curves were carried out using a PPMS-9 (Quantum Design, USA) vibrating sample magnetometer (VSM) and the results were shown in Fig. 8. The saturation magnetisation values of $Fe_3O_4$, $Fe_3O_4$/Au, $Fe_3O_4$/Au/$SiO_2$, $Fe_3O_4$/Au/$SiO_2$/PNIPAM, and $Fe_3O_4$/Au/void/PNIPAM were measured to be 66.5, 49.7, 32.4, 26.2, and 34.5 emu/g, respectively. The zero remanence or coercivity and the reversible hysteresis loops indicated the superparamagnetic nature of each sample [33], which indicated that the magnetite particles are composed of ultrafine nanocrystals with size in the 10–20 nm range [34]. As a result of the well-retained high magnetic intensity, the $Fe_3O_4$/Au/void/PNIPAM microspheres can be easily separated from the mixture in less than few minutes by simply using a magnet.

3.4. Catalytic activities of the yolk–shell microspheres: The AuNPs catalysed reduction of 4-NP by $NaBH_4$ to 4-AP was chosen as a model reaction [10, 35] to test the temperature switch on/off activities of the yolk–shell microspheres under different reaction temperatures (25, 32, 45, 55°C). When a trace amount of the yolk–shell microspheres were introduced into the system, the bright-yellow solution gradually faded. When the cross-linking degree of PNIPAM shell was 10% (v/v), the conversion of 4-NP was monitored by UV–vis spectroscopy (Fig. 9). The absorption peak at 400 nm of 4-NP gradually decreased and the absorption peak at 300 nm of 4-AP [10] increased at all temperatures. When the environmental temperature was 25°C, nearly all of 4-NP were converted into 4-AP about 6 min (Fig. 9*a*). When the temperature was 32°C, the full reaction time was increased to 10 min (Fig. 9*b*). While the circumstance temperature was 45 and 55°C, the full conversion time was more than 30 min (Figs. 9*c* and *d*). This decrease of reaction rate following the increase of temperature was originated from the temperature-dependent swelling transition property of the PNIPAM which had a well-known phase transition temperature (LCST) at around 32°C in aqueous media [3]. Under

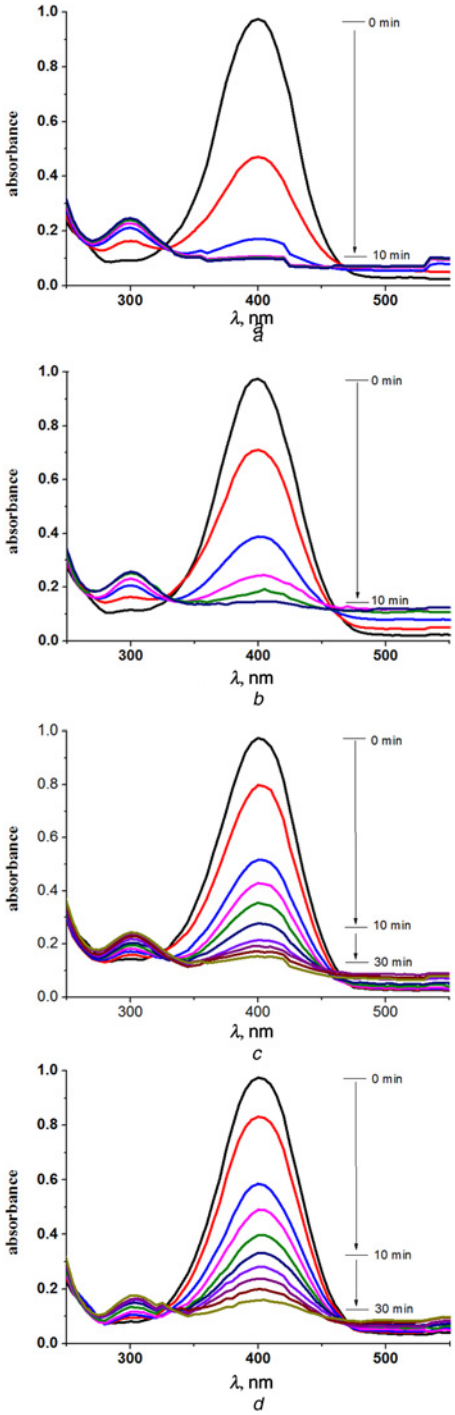


**Fig. 9** *UV–vis spectra of the reduction of 4-NP using yolk–shell microspheres with 10% cross-linking degree at different temperatures*
*a* 25°C
*b* 32°C
*c* 45°C
*d* 55°C

the LCST, PNIPAM chains were hydrophilic, which resulted in a swelling state and opening pores of PNIPAM shell. Therefore, the 4-NP molecules could across the shell, approach the core of yolk–shell microsphere, and be catalysed by the AuNPs. However, above the LCST, the hydrophobic and shrinking sate of PNIPAM shell could lead to the close of pores of PNIPAM and decrease of reaction rate, gradually.

When the cross-linking degree of PNIPAM shell increased to 20% (v/v), the reaction rate slowed in all cases (Fig. 10), especially

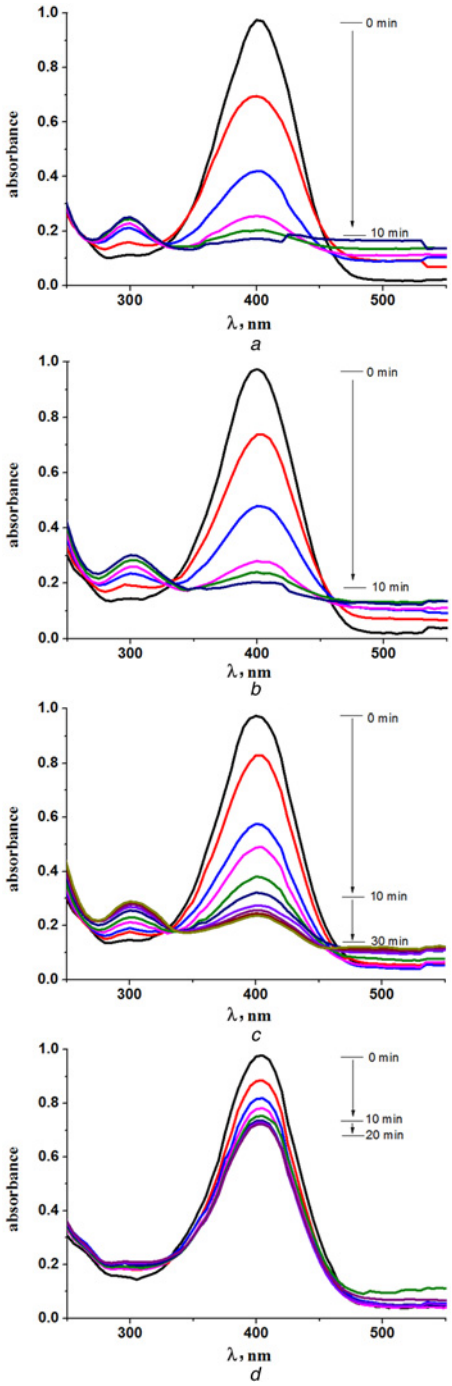


**Fig. 10** *UV–vis spectra of the reduction of 4-NP using yolk–shell microspheres with 20% cross-linking degree at different temperatures*
*a* 25°C
*b* 32°C
*c* 45°C
*d* 55°C

when the temperature was 55°C, the reaction reached equilibrium about 20min and only 26% of 4-NP was reduced (Fig. 10*c*), which indicated that the increase of cross-linking degree from 10 to 20% could result in an obvious increase of temperature switch because a reasonable rigidity of polymeric chains could result in a suitable switch and mass transfer ability of PNIPAM [18].

Considering the concentration of $NaBH_4$ was much higher than that of 4-NP and could be considered as a constant during the reaction period [35], the reduction process should be regarded as a first-order reaction with regard to 4-NP, and thus the relationship

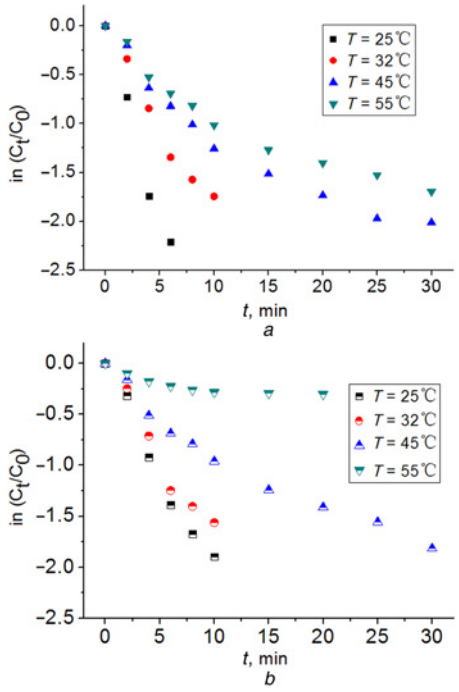


**Fig. 11** *Relationship between ln($C_t$/$C_0$) and reaction time (t) under different temperatures by the two kinds of yolk–shell microspheres with different cross-linking degree of*
*a* 10%
*b* 20%

between In($C_t$/$C_0$) and reaction time ($t$) would conform to a linear form, wherein $C_t$ denotes the concentration of 4-NP at time $t$ and $C_0$ denotes its initial concentration, the $C_t$/$C_0$ was directly measured from the relative intensity of the respective absorbance ($A_t$/$A_0$). To further study the temperature-responsive catalytic performance, the relationship between In($C_t$/$C_0$) and reaction time ($t$) under different temperatures by the two kinds of yolk–shell microspheres with different cross-linking degrees (10 and 20%) were shown in Fig. 11 and the rate constant ($K$) was calculated from the rate equation

$$\ln\left(\frac{C_t}{C_0}\right) = -kt \tag{1}$$

The results of Fig. 11 indicated that all these plots matched the first-order reaction kinetics before the reactions reached the equilibrium points and the increase of temperature would lead to the decrease of the reaction rate in both cases. The $K$ value had an obvious decrease at the low temperature region (25–32°C) when the cross-linking degree was 10%, while it decreased greatly at the high temperature region (45–55°C) when the cross-linking degree was 20%. In the whole reaction, two key factors, hydrophilicity and rigidity of PNIPAM chains, greatly influenced the mass transfer ability of PNIPAM shells because the cross-linking would increase the hydrophobicity and rigidity of PNIPAM shells. The PNIPAM shells with lower cross-linking degree should had a better hydrophilicity and a lower rigidity, which indicated that the mass transfer of small molecules was dominated by the hydrophilicity of PNIPAM shells at a lower cross-linking degree and temperature ($T$ < LCST); whereas the mass transfer was dominated by the rigidity of PNIPAM shells at a higher cross-linking degree and temperature ($T$ > LCST). Therefore, the yolk–shell microspheres of 20% cross-linking degree exhibited a good temperature switch ability.

3.5. Reusability of the yolk–shell microspheres.: Recyclability of magnetic nanoparticles-based heterogeneous catalysts was




doi: 10.1049/mnl.2015.0435

**Table 1** Comparison of kinetic constant ($K$) of 4-NP reduction under different temperatures

| Temperature, °C | $K_{10\%}$, $min^{-1}$ | $K_{20\%}$, $min^{-1}$ |
|---|---|---|
| 25 | 0.38 | 0.20 |
| 32 | 0.19 | 0.17 |
| 45 | 0.10 | 0.06 |
| 55 | 0.06 | 0.02 |

**Table 2** Cycle performance of the yolk–shell microspheres with 20 % cross-linking degree at 25°C

| Cycle times | 1 | 2 | 3 | 4 | 5 | 6 |
|---|---|---|---|---|---|---|
| Catalytic activity, % | 100 | 89.4 | 85.5 | 79.3 | 76.3 | 74.6 |

important for their practical application. The reusability of the yolk–shell microspheres of 20% cross-linking degree were investigated and listed in Table 2.

After six cycles, the yolk–shell microspheres still had the temperature switch on/off character and the catalytic activity of yolk–shell microspheres was about 74.6%, which indicated that these yolk–shell microspheres had a good cycle performance. The decrease of catalytic activity could be ascribed to the dissociation of $Fe_3O_4$/Au cores during the catalytic processes because each $Fe_3O_4$ nanoparticle was an aggregation of $Fe_3O_4$ nanocrystals about 13 nm [36]. Therefore, the AuNPs could be released from the yolk–shell.

**4. Conclusion:** In this Letter, a yolk–shell microsphere with a movable core in large diameter was synthesised when thermoresponsive PNIPAM was as the shell and $Fe_3O_4$ self-assembled AuNPs as the core. The yolk–shell structure was researched by TEM, VSM, FT-IR and so on. The temperature switch on/off character was investigated by the reduction of 4-NP to 4-AP as the model reaction and the results suggested that the cross-linking degree, hydrophilicity and rigidity of PNIPAM chains greatly influenced the mass transfer ability and catalytic activity of the yolk–shell microspheres. When the circumstance temperature increased, all reaction rates slowed because of the thermoresponsive PNIPAM. Moreover, at a lower cross-linking degree (10%) and temperature ($T$ < LCST), the mass transfer of 4-NP and catalytic activity of the yolk–shell microspheres were dominated by the hydrophilicity of PNIPAM shells, while those of yolk–shell microspheres were dominated by the rigidity of PNIPAM shells at a higher cross-linking degree (20%) and temperature ($T$ > LCST).

**5. Acknowledgments:** This work was supported by the National Natural Science Foundation of China (nos. 21172171 and 21206124), Natural Science Foundation of Tianjin (no. 15JCYBJC20500).

## 6 References

[1] Sarti S., Bordi F.: 'Polymeric hollow micro and nanospheres for biotechnological applications: a focused review', *Mat. Lett.*, 2013, **109**, pp. 134–139
[2] Xu S.B., Wang J.X., Cheng S.F., *ET AL.*: 'Control synthesis and formation mechanism of sphere-like titanium dioxide', *Micro Nano Lett.*, 2015, **10**, pp. 23–27
[3] Fuji M., Takai C., Virtudazo R.V.R.: 'Development of new templating approach for hollow nanoparticles and their applications', *Adv. Powder Technol.*, 2014, **25**, pp. 91–100
[4] He M.Q., Sun K.Y., Xia J.X., *ET AL.*: 'Reactable ionic liquid-assisted solvothermal synthesis of flower-like bismuth oxybromide microspheres with highly visible-light photocatalytic performances', *Micro Nano Lett.*, 2013, **8**, pp. 450–454
[5] Zhang M.C., Lan Y., Wang D., *ET AL.*: 'Synthesis of polymeric yolk-shell microspheres by seed emulsion polymerization', *Macromolecules*, 2011, **44**, pp. 842–847
[6] Hong Y.J., Kang Y.C.: 'General formation of tin nanoparticles encapsulated in hollow carbon spheres for enhanced lithium storage capability', *Small*, 2015, **11**, pp. 2157–2163
[7] Dahl M., Liu Y.D., Yin Y.D.: 'Composite titanium dioxide nanomaterials', *Chem. Rev.*, 2014, **114**, pp. 9853–9889
[8] Carenco S., Portehault D., Boissière C., *ET AL.*: 'Nanoscaled metal borides and phosphides: recent developments and perspectives', *Chem. Rev.*, 2013, **113**, pp. 7981–8065
[9] Du P.C., Liu P.: 'Novel smart yolk/shell polymer microspheres as a multiply responsive cargo delivery system', *Langmuir*, 2014, **30**, pp. 3060–3068
[10] Wang S.N., Zhang M.C., Zhang W.Q.: 'Yolk-shell catalyst of single Au nanoparticle encapsulated within hollow mesoporous silica microspheres', *ACS Catalysis*, 2011, **1**, pp. 207–211
[11] Liu L., Du P.C., Zhao X.B., *ET AL.*: 'Independent temperature and pH dual-stimuli responsive yolk/shell polymer microspheres for controlled release: structural effect', *Eur. Polym. J.*, 2015, **69**, pp. 540–551
[12] Liu G.Y., Ji H.F., Yang X.L., *ET AL.*: 'Synthesis of an Au/silica/polymer trilayer composite and the corresponding hollow polymer microsphere with a movable Au core', *Langmuir*, 2008, **24**, pp. 1019–1025
[13] Lu A.H., Salabas E.L., Schüth F.: 'Magnetic nanoparticles: synthesis, protection, functionalization, and application', *Angew. Chem., Int. Ed.*, 2007, **46**, pp. 1222–1244
[14] Zhang W.M., Hu J.S., Guo Y.G., *ET AL.*: 'Tin-nanoparticles encapsulated in elastic hollow carbon spheres for high-performance anode material in lithium-ion batteries', *Adv. Mater.*, 2008, **20**, pp. 1160–1160
[15] Hong Y.J., Son M.Y., Park B.K., *ET AL.*: 'One-Pot synthesis of yolk-shell materials with single, binary, ternary, quaternary, and quinary systems', *Small*, 2013, **9**, pp. 2224–2227
[16] Güttel R., Paul M., Schüth F.: 'Ex-post size control of high-temperature-stable yolk-shell Au, @ $ZrO_2$ catalysts', *Chem. Commun.*, 2010, **46**, pp. 895–897
[17] Lapeyre V., Renaudie N., Dechezelles J.F., *ET AL.*: 'Multiresponsive hybrid microgels and hollow capsules with a layered structure', *Langmuir*, 2009, **25**, pp. 4659–4667
[18] Li G.L., Lei C.L., Wang C.H., *ET AL.*: 'Narrowly dispersed double-walled concentric hollow polymeric microspheres with independent pH and temperature sensitivity', *Macromolecules*, 2008, **41**, pp. 9487–9490
[19] Yang S.M., Kim S.H., Lim J.M., *ET AL.*: 'Synthesis and assembly of structured colloidal particles', *J. Mater. Chem.*, 2008, **18**, pp. 2161–2284
[20] Yao T.J., Cui T.Y., Fang X., *ET AL.*: 'Preparation of yolk/shell $Fe_3O_4$@polypyrrole composites and their applications as catalyst supports', *Chem. Eng. J.*, 2013, **225**, pp. 230–236
[21] Nabid M.R., Bide Y., Ghalavand N.: 'Copper (I) ion stabilized on $Fe_3O_4$-core ethylated branched polyethyleneimine-shell as magnetically recyclable catalyst for ATRP reaction', *J. Appl. Polym, Sci.*, 2015, **132**, pp. 42337
[22] Yang Q.F., Dai Z., Guo W.J., *ET AL.*: 'Preparation and catalytic performance of temperature-responsive cell-like particles', *Pak. J. Pharm. Sci.*, 2014, **27**, pp. 1611–1614
[23] Liu J., Sun Z.K., Deng Y.H., *ET AL.*: 'Highly water-dispersible biocompatible magnetite particles with low cytotoxicity stabilized by citrate groups', *Angew. Chem., Int. Ed.*, 2009, **48**, pp. 5875–5879
[24] Fren G.: 'Preparation of gold dispersions of varying particle size: Controlled nucleation for the regulation of the particle size in monodisperse gold suspensions', *Nat. Phys. Sci.*, 1973, **241**, pp. 20–22
[25] Graf C., Vossen D.L.J., Imhof A., *ET AL.*: 'A general method to coat colloidal particles with silica', *Langmuir*, 2003, **19**, pp. 6693–6700
[26] Luo B., Song X.J., Zhang F., *ET AL.*: 'Multi-functional thermosensitive composite microspheres with high magnetic susceptibility based on magnetite colloidal nanoparticle clusters', *Langmuir*, 2010, **26**, pp. 1674–1679
[27] Liz-Marzán L.M., Giersig M., Mulvaney P.: 'Synthesis of nanosized gold-silica core-shell particles', *Langmuir*, 1996, **12**, pp. 4329–4335
[28] Xu Z.F., Ahsan Uddin K.M., Kamra T., *ET AL.*: 'Fluorescent boronic acid polymer grafted on silica particles for affinity separation of saccharides', *ACS Appl. Mater. Interf.*, 2014, **6**, pp. 1406–1414
[29] Moraes J., Ohno K., Maschmeyer T., *ET AL.*: 'Synthesis of silica-polymer core–shell nanoparticles by reversible addition-fragmentation chain transfer polymerization', *Chem. Commun.*, 2013, **49**, pp. 9077–9088

[30] Sun L., Zhang X.G., Zheng C., *ET AL.*: 'A pH gated, glucose-sensitive nanoparticle based on worm-like mesoporous silica for controlled insulin release', *J. Phys. Chem. B*, 2013, **117**, pp. 3852–3860
[31] Bourgeat-Lami E., Lang J.: 'Encapsulation of inorganic particles by dispersion polymerization in polar media. 1. Silica nanoparticles encapsulated by polystyrene', *J. Colloid Interf. Sci.*, 1998, **197**, pp. 293–308
[32] Li G.L., Liu G., Kang E.T., *ET AL.*: 'pH-responsive hollow polymeric microspheres and concentric hollow silica microspheres from silica-polymer core-shell microspheres', *Langmuir*, 2008, **24**, pp. 9050–9055
[33] Xu H., Cui L.L., Tong N.H., *ET AL.*: 'Development of high magnetization $Fe_3O_4$/polystyrene/silica nanospheres via combined miniemulsion/emulsion polymerization', *J. Am. Chem. Soc.*, 2006, **128**, pp. 15582–15583
[34] Wunder S., Polzer F., Lu Y., *ET AL.*: 'Kinetic analysis of catalytic reduction of 4-nitrophenol by metallic nanoparticles immobilized in spherical polyelectrolyte brushes', *J. Phys. Chem. C*, 2010, **114**, pp. 8814–8820
[35] Lin F-H., Doong R.-A.: 'Bifunctional Au-$Fe_3O_4$ heterostructures for magnetically recyclable catalysis of nitrophenol reduction', *J. Phys. Chem. C*, 2011, **115**, pp. 6591–6598
[36] Deng Y.H., Cai Y., Sun Z.K., *ET AL.*: 'Multifunctional mesoporous composite microspheres with well-designed nanostructure: A highly integrated catalyst system', *J. Am. Chem. Soc.*, 2010, **132**, pp. 8466–8473




doi: 10.1049/mnl.2015.0435